Calculating quasinormal modes of extremal and nonextremal Reissner-Nordström black holes with the continued fraction method

Ramin G. Daghigh[1], Michael D. Green[2], and Jodin C. Morey[3]

[1]*Natural Sciences Department, Metropolitan State University, Saint Paul, Minnesota 55106, USA*
[2]*Mathematics and Statistics Department, Metropolitan State University, Saint Paul, Minnesota 55106, USA*
[3]*School of Mathematics, University of Minnesota, Minneapolis, Minnesota 55455, USA*

We use the numerical continued fraction method to investigate the quasinormal mode spectra of extremal and nonextremal Reissner-Nordström black holes in the low- and intermediate-damping regions. In the extremal case, we develop techniques that significantly expand the calculated spectrum from what had previously appeared in the literature. This allows us to determine the asymptotic behavior of the extremal spectrum in the high-damping limit, where there are conflicting published results. Our investigation further supports the idea that the extremal limit of the nonextremal case, where the charge approaches the mass of the black hole in natural units, leads to the same vibrational spectrum as in the extremal case despite the qualitative differences in their topology. In addition, we numerically explore the quasinormal mode spectrum for a Reissner-Nordström black hole in the small-charge limit.

I. INTRODUCTION

Natural vibrational modes, also called quasinormal modes (QNMs), of black holes have attracted a great deal of attention since the first detection of gravitational waves emitted from a binary black hole merger [1]. There also have been efforts in establishing a link between QNMs and the quantum structure of a black hole spacetime. See, for example, Refs. [2–4].

In this paper, we focus on the QNMs of extremal and nonextremal Reissner-Nordström (RN) black holes with charge q and mass M. Extremal black holes, when $q = M$ using units where $G = c = k_e = 1$, hold an important and controversial status in black hole physics. Traditionally, these black holes were believed to be a limiting case of nonextremal black holes [5]. This traditional view was challenged by Hawking and Horowitz in [6] based on the fact that the topologies of the extremal and nonextremal black holes have qualitative differences. Due to these differences, the authors of [6,7] argued that extremal RN black holes have zero entropy with no definite temperature despite having a nonzero horizon area. Extremal black holes are also important in the context of supergravity theories [8].

In [9], Onozawa *et al.* numerically computed the least-damped modes for four-dimensional extremal RN black holes. They found that the QNM spectra of gravitational waves with multipole index ℓ and electromagnetic waves with multipole index $\ell - 1$ coincide.[1] Based on this observation, the authors of [10] conjectured that the modes of different perturbations can be matched because of the supersymmetry transformations in the extremal solution. In [11], Berti was able to extend the numerical calculation of [9] to include higher-damped modes. Berti's results show that the extremal RN QNM spectrum has a similar pattern to the Schwarzschild case. As the damping increases, the oscillation frequency seems to approach the same constant value as in Schwarzschild black holes—i.e.,

$$\omega_R \underset{|\omega_I| \to \infty}{\to} \frac{\ln(3)}{8\pi M}, \qquad (1.1)$$

where ω_R represents the real part of the vibration frequency of the QNM ω, and ω_I is the imaginary part that determines the damping rate. This result seems to be compatible with the extremal limit, where $q \to M$, of the nonextremal RN QNM spectrum which was derived in [12] for the highly damped limit ($|\omega_I| \to \infty$). Unfortunately, the numerical method in [11] is unstable after approximately 20 roots. Therefore, one cannot verify the limit in Eq. (1.1). It is suggested in [12] that since the topology of the Stokes/anti-Stokes lines for the

---

[1]Electromagnetic and gravitational waves in the RN black hole are coupled. Here, electromagnetic (gravitational) refers to perturbations that reduce to pure electromagnetic (gravitational) perturbations in the zero-charge limit.

extremal RN black hole is different from that in the nonextremal case, the QNMs for these black holes would require a separate analysis. Following this suggestion, the authors of [13,14] have attempted to explicitly calculate the highly damped QNM frequency of extremal RN black holes using the monodromy method of [15]. Neither of the analytic results in [13,14] matches the QNM spectrum of the extremal limit of the nonextremal case. Therefore, they contradict the numerical results provided by Berti in [11]. In [16], two of us used the topology of anti-Stokes lines presented in [14] to show that in the highly damped limit, a particular path along the anti-Stokes lines will lead to results in agreement with Berti's numerical calculation in [11], and with the extremal limit of the nonextremal case derived in [12]. A geometric treatment of the extremal and near-extremal cases in [17] also leads to similar conclusions. In this paper, we extend the numerical results of Berti to higher-overtone QNMs to show that the QNM spectrum of the extremal case matches the extremal limit.

Another issue that we examine in this paper is about the transition between intermediate- and high-damping regions of the QNM spectrum of RN black holes in the small-charge limit ($q \to 0$). It was shown first by Motl and Neitzke [15] and then confirmed by Andersson and Howls [12] that for RN black holes, the real part of the highly damped QNM frequency in four dimensions approaches $\ln(5)/(8\pi M)$ as the charge goes to zero. The general validity of this result was verified by Natario and Schiappa [14], who calculated RN highly damped spectra in arbitrary spacetime dimensions. The apparent contradiction between the zero-charge limit of the RN case and the Schwarzschild value was explained heuristically by the authors of [12]. They noted that, while $\ln(5)/(8\pi M)$ represents the correct RN result for very high damping, one expects an intermediate range of damping in which one finds the Schwarzschild value of $\ln(3)/(8\pi M)$ for ω_R. Order-of-magnitude arguments suggest this range in four spacetime dimensions to be

$$1 \ll |\omega|^2 M^2 \ll M^8/q^8. \qquad (1.2)$$

In [18], the authors use a combination of analytical and numerical techniques to analyze the limit of large but finite damping where the Schwarzschild limit is approached. For four and five spacetime dimensions, the authors of [18] explicitly calculate the spectrum in the transition region from $\ln(3 + 4\cos(\frac{d-3}{2d-5}\pi))/(8\pi M)$, in d spacetime dimensions, for very large damping to the Schwarzschild value of $\ln(3)/(8\pi M)$. Based on this work, the real frequency does not interpolate smoothly between the two values. Instead, there is a critical value of the damping at which the Stokes/anti-Stokes lines change topology and the real part of the frequency dips to zero. This behavior seems to resemble the algebraically special frequencies that mark the onset of the high-damping regime.

The paper is organized as follows: In Sec. II, we describe the general formalism and the continued fraction method for the nonextremal case. In Sec. III, we describe numerical methods to address the extremal case. In Sec. IV, we report and discuss the results. Finally, in Sec. V, we end the paper with some concluding remarks.

II. GENERAL FORMALISM

Various classes of nonrotating black hole metric perturbations are governed generically by a Schrödinger-like wave equation of the form

$$\frac{d^2\psi}{dr_*^2} + [\omega^2 - V(r)]\psi = 0, \qquad (2.1)$$

where $V(r)$ is the QNM potential. In this paper, we assume that the perturbations depend on time as $e^{-i\omega t}$. Consequently, in order to have damping, the imaginary part of ω must be negative. The tortoise coordinate r_* is defined by

$$dr_* = \frac{dr}{f(r)}, \qquad (2.2)$$

where the metric function, $f(r)$, for the Reissner-Nordström spacetime is given by

$$f(r) = 1 - \frac{2M}{r} + \frac{q^2}{r^2}. \qquad (2.3)$$

Combining the above two equations gives us the tortoise coordinate

$$r_* = r + \frac{r_+^2}{r_+ - r_-}\ln(r - r_+) - \frac{r_-^2}{r_+ - r_-}\ln(r - r_-), \qquad (2.4)$$

where $r_\pm = (M \pm \sqrt{M^2 - q^2})$ are the roots of the metric function that determine the locations of the inner (Cauchy) and outer (event) horizons. M is the ADM mass of the black hole, and q is the charge. The effective potential[2] in Eq. (2.1) is

$$V_s(r) = f(r)\left[\frac{\ell(\ell+1)}{r^2} - \frac{\beta_s}{r^3} + \frac{4q^2}{r^4}\right], \qquad (2.5)$$

where ℓ is the multipole number, $s = 1$ corresponds to perturbations that reduce to purely electromagnetic perturbations as $q \to 0$ (hereafter "electromagnetic" for brevity), $s = 2$ corresponds to perturbations that reduce to purely

---

[2]Here we only consider axial perturbations, since the polar perturbations can be obtained from axial perturbations using the Chandrasekhar transformation [19].

axial gravitational perturbations as $q \to 0$ (hereafter "gravitational" for brevity), and

$$\beta_s = 3M + (-1)^s \sqrt{9M^2 + 4q^2(\ell - 1)(\ell + 2)}. \quad (2.6)$$

The effective potential is zero at the event horizon $(r \to r_+)$ and at spatial infinity $(r \to \infty)$. The QNMs are obtained using the boundary conditions in which the asymptotic behavior of the solutions is

$$\psi(r) \approx \begin{cases} e^{-i\omega r_*} & \text{as } r_* \to -\infty \\ e^{i\omega r_*} & \text{as } r_* \to \infty \end{cases}, \quad (2.7)$$

representing ingoing waves at the event horizon and outgoing waves at infinity.

We can write the solution to the wave equation (2.1), with the desired behavior at the boundaries, in the form

$$\psi(r) = \frac{r_+ e^{-2i\omega r_+} (r_+ - r_-)^{-2i\omega-1} (r - r_-)^{1+i\omega} e^{i\omega r}}{r}$$
$$\times u^{-i\omega r_+^2/(r_+-r_-)} \sum_{n=0}^{\infty} a_n u^n, \quad (2.8)$$

where $u = (r - r_+)/(r - r_-)$. Inserting (2.8) into the wave equation (2.1) leads to a four-term recurrence relation:

$$\alpha_1 a_1 + \beta_1 a_0 = 0, \quad (2.9)$$

$$\alpha_2 a_2 + \beta_2 a_1 + \gamma_2 a_0 = 0, \quad (2.10)$$

$$\alpha_n a_n + \beta_n a_{n-1} + \gamma_n a_{n-2} + \delta_n a_{n-3} = 0, \quad (2.11)$$

where $n = 3, 4, 5, \ldots$, and a_0 is a constant which we can take to be 1. The coefficients in the above recurrence relation, which are functions of ω, are given in [20] for both gravitational and electromagnetic perturbations. The QNMs are the values of ω that satisfy the above four-term recurrence relation for all n. The recurrence relation (2.11) can be reduced to a three-term recurrence relation,

$$\alpha_n' a_n + \beta_n' a_{n-1} + \gamma_n' a_{n-2} = 0, \quad (2.12)$$

using Gaussian elimination. For details, see Ref. [20].

Following Leaver in [21], this three-term recurrence relation gives a continued fraction equation

$$\beta_1' = \frac{\alpha_1' \gamma_2'}{\beta_2' - \frac{\alpha_2' \gamma_3'}{\beta_3' - \cdots}}$$
$$= \frac{\alpha_1' \gamma_2'}{\beta_2'-} \frac{\alpha_2' \gamma_3'}{\beta_3'-} \frac{\alpha_3' \gamma_4'}{\beta_4'-} \cdots, \quad (2.13)$$

which can be solved for ω. For higher-overtone QNMs, we use inversions of (2.13) as described in [21]. To evaluate the continued fraction numerically, we truncate it at some point and approximate the tail-end using Nollert's technique [22].

In the extremal case, where $q = M$ $(r_+ = r_-)$, we have a different topology that requires a new approach suggested by [9]. We review the extremal case in the next section.

III. THE EXTREMAL CASE

In the extremal case, where $M = q$, the tortoise coordinate becomes

$$r_* = r - \frac{M^2}{r - M} + 2M \ln(r - M). \quad (3.1)$$

This leads to irregular singularities of the radial wave equation at the event horizon, $r = M$, and at infinity. Leaver's method would be to expand the solution around the horizon using $u = (r - M)/r$ in (2.8). However, since $r = M$ is an irregular singularity of the differential equation, this will not work, since the series will not converge. Onozawa *et al.* [9] get around this issue by using $u = (r - 2M)/r$ instead. With this choice, the horizon is at $u = -1$ and infinity is at $u = 1$. After substituting $\sum_n a_n u^n$ into the wave equation, we obtain a five-term recurrence relation for the a_n with coefficients α_n, β_n, γ_n, δ_n, and ϵ_n. Now, the convergences of the wave function [Eq. (17) in [9]] at the event horizon and at infinity is equivalent to the convergences of $\sum(-1)^n a_n$ and $\sum a_n$, respectively. This is the same as requiring $\sum_{n \text{ odd}} a_n$ and $\sum_{n \text{ even}} a_n$ to converge. Onozawa shows that the $a_{n \text{ odd}}$ themselves satisfy a five-term recurrence relation with coefficients $\hat{\alpha}_n$, $\hat{\beta}_n$, $\hat{\gamma}_n$, $\hat{\delta}_n$, and $\hat{\epsilon}_n$, as do the $a_{n \text{ even}}$ with coefficients $\bar{\alpha}_n$, $\bar{\beta}_n$, $\bar{\gamma}_n$, $\bar{\delta}_n$, and $\bar{\epsilon}_n$. These coefficients are related by the following equation [9]:

$$\frac{a_3}{a_1} = \frac{-\frac{\alpha_5}{\bar{\alpha}_2''} \bar{\gamma}_2'' + \epsilon_5 + \left(-\frac{\alpha_5}{\bar{\alpha}_2''} \bar{\beta}_2'' + \gamma_5\right) \frac{a_4}{a_2}}{\alpha_3 \frac{a_4}{a_2} + \gamma_3 - \epsilon_3 \frac{\alpha_1}{\gamma_1}}, \quad (3.2)$$

where a_4/a_2 and a_3/a_1 can be written as continued fractions of the form

$$\frac{a_4}{a_2} = \frac{-\bar{\gamma}_2''}{\bar{\beta}_2'' - \frac{\bar{\alpha}_2'' \bar{\gamma}_3''}{\bar{\beta}_3'' - \frac{\bar{\alpha}_3'' \bar{\gamma}_4''}{\bar{\beta}_4'' - \cdots}}}, \quad (3.3)$$

$$\frac{a_3}{a_1} = \frac{-\hat{\gamma}_1''}{\hat{\beta}_1'' - \frac{\hat{\alpha}_1'' \hat{\gamma}_2''}{\hat{\beta}_2'' - \frac{\hat{\alpha}_2'' \hat{\gamma}_3''}{\hat{\beta}_3'' - \cdots}}}. \quad (3.4)$$

Here, $''$ indicates the coefficients obtained when the even and odd recurrence relations are reduced to three terms; see Ref. [9].[3]

The solutions ω to Eq. (3.2) are the QNMs. However, using this equation, we are only able to find a few of the solutions. Typically, when working with continued fraction equations, it is possible to form inversions that make certain roots more numerically stable. Therefore, the inversion allows one to find other roots. For most black holes, the QNM equation involves one continued fraction, whereas here there are two, a_4/a_2 and a_3/a_1. To be able to calculate the QNMs, we consider two different inversion methods. The first method involves evaluating one continued fraction (either a_4/a_2 or a_3/a_1) to a fixed depth and inverting the other one. In the second method, we invert both simultaneously. We briefly explain these two methods below.

In the first method, we invert the following equation:

$$\frac{-\hat{\gamma}_1''}{\hat{\beta}_1'' - \dfrac{\hat{\alpha}_1''\hat{\gamma}_2''}{\hat{\beta}_2'' - \dfrac{\hat{\alpha}_2''\hat{\gamma}_3''}{\hat{\beta}_3'' - \cdots}}} = \mathcal{F}(\omega), \qquad (3.5)$$

where $\mathcal{F}(\omega)$ is the right-hand side of (3.2). We call (3.5) the first inversion. The nth inversion, for $n = 2, 3, \ldots$, of (3.5), is defined to be

$$\hat{\beta}_n'' - \frac{\hat{\alpha}_{n-1}''\hat{\gamma}_n''}{\hat{\beta}_{n-1}''-}\frac{\hat{\alpha}_{n-2}''\hat{\gamma}_{n-1}''}{\hat{\beta}_{n-2}''-}\cdots\frac{\hat{\alpha}_1''\hat{\gamma}_2''}{\hat{\beta}_1''-}\frac{-\hat{\gamma}_1''}{\mathcal{F}(\hat{\omega})}$$
$$= \frac{\hat{\alpha}_n''\hat{\gamma}_{n+1}''}{\hat{\beta}_{n+1}''-}\frac{\hat{\alpha}_{n+1}''\hat{\gamma}_{n+2}''}{\hat{\beta}_{n+2}''-}\frac{\hat{\alpha}_{n+2}''\hat{\gamma}_{n+3}''}{\hat{\beta}_{n+3}''-}\cdots. \qquad (3.6)$$

For each inversion, we find a number of QNMs. A rough rule of thumb is that the nth QNM, ω_n, is the most stable solution of the nth inversion. Thus, we are able to find a large number of roots by taking more and more inversions. Alternatively, we can first solve (3.2) for a_4/a_2 and repeat the above procedure.

Whichever continued fraction is inverted, we find the same roots up to roughly ω_{200}. Interestingly, after $n \approx 200$, the inversions of Eq. (3.5) only give every other root. Similarly, the equation we get by first solving for a_4/a_2 and then inverting also starts to give us every other root. Conveniently, the two inversion methods are complementary in finding the roots that are missing in the other one. Thus, we are able to find roots up to roughly ω_{1000}.

In the second method, we simultaneously invert both continued fractions, a_3/a_1 and a_4/a_2. To abbreviate the procedure, we rewrite Eq. (3.2) as

---

[3]Note that the exact form of these coefficients in [9] requires $M = 1$.

$$\mathcal{O}_1 = \frac{-\frac{\alpha_5}{\bar{\alpha}_2''}\bar{\gamma}_2'' + \epsilon_5 + \left(-\frac{\alpha_5}{\bar{\alpha}_2''}\bar{\beta}_2'' + \gamma_5\right)\mathcal{E}_1}{\alpha_3\mathcal{E}_1 + \gamma_3 - \epsilon_3\frac{\alpha_1}{\gamma_1}}. \qquad (3.7)$$

We can put this in the form

$$A_1\mathcal{O}_1 + B_1\mathcal{E}_1 + C_1\mathcal{E}_1\mathcal{O}_1 + D_1 = 0, \qquad (3.8)$$

where

$$\mathcal{E}_1 = \frac{a_4}{a_2} = \frac{-\bar{\gamma}_2''}{\bar{\beta}_2'' - \dfrac{\bar{\alpha}_2''\bar{\gamma}_3''}{\bar{\beta}_3'' - \cdots}}, \qquad (3.9)$$

$$\mathcal{O}_1 = \frac{a_3}{a_1} = \frac{-\hat{\gamma}_1''}{\hat{\beta}_1'' - \dfrac{\hat{\alpha}_1''\hat{\gamma}_2''}{\hat{\beta}_2'' - \cdots}}, \qquad (3.10)$$

$$A_1 = \gamma_3 - \frac{\alpha_1\epsilon_5}{\gamma_1}, \qquad (3.11)$$

$$B_1 = \frac{\alpha_5}{\bar{\alpha}_2''}\bar{\beta}_2'' - \gamma_5, \qquad (3.12)$$

$$C_1 = \alpha_3, \qquad (3.13)$$

$$D_1 = \frac{\alpha_5}{\bar{\alpha}_2''}\bar{\gamma}_2'' - \epsilon_5. \qquad (3.14)$$

We create "inversions" of (3.8) by multiplying by the denominator of the continued fractions of $\mathcal{E}_1$ and $\mathcal{O}_1$. Repeating this process, the nth inversion will have the form

$$A_n\mathcal{O}_n + B_n\mathcal{E}_n + C_n\mathcal{E}_n\mathcal{O}_n + D_n = 0, \qquad (3.15)$$

where

$$\mathcal{E}_n = \bar{\beta}_{n+1}'' - \frac{\bar{\alpha}_{n+1}''\bar{\gamma}_{n+2}''}{\bar{\beta}_{n+2}'' - \dfrac{\bar{\alpha}_{n+2}''\bar{\gamma}_{n+3}''}{\bar{\beta}_{n+3}'' - \cdots}}, \qquad (3.16)$$

$$\mathcal{O}_n = \hat{\beta}_n'' - \frac{\hat{\alpha}_n''\hat{\gamma}_{n+1}''}{\hat{\beta}_{n+1}'' - \dfrac{\hat{\alpha}_{n+1}''\hat{\gamma}_{n+2}''}{\hat{\beta}_{n+2}'' - \cdots}}, \qquad (3.17)$$

$$A_2 = -\bar{\gamma}_2''B_1, \qquad (3.18)$$

$$B_2 = -\hat{\gamma}_1''A_1, \qquad (3.19)$$

$$C_2 = D_1, \qquad (3.20)$$

$$D_2 = \hat{\gamma}_1''\bar{\gamma}_2''C_1, \qquad (3.21)$$

$$A_n = -\bar{\alpha}_{n-1}''\bar{\gamma}_n''(B_{n-1} + \hat{\beta}_{n-2}''C_{n-1}), \quad n > 2, \qquad (3.22)$$

$$B_n = \hat{\alpha}_{n-2}''\hat{\gamma}_{n-1}''(A_{n-1} + \bar{\beta}_{n-1}''C_{n-1}), \quad n > 2, \qquad (3.23)$$
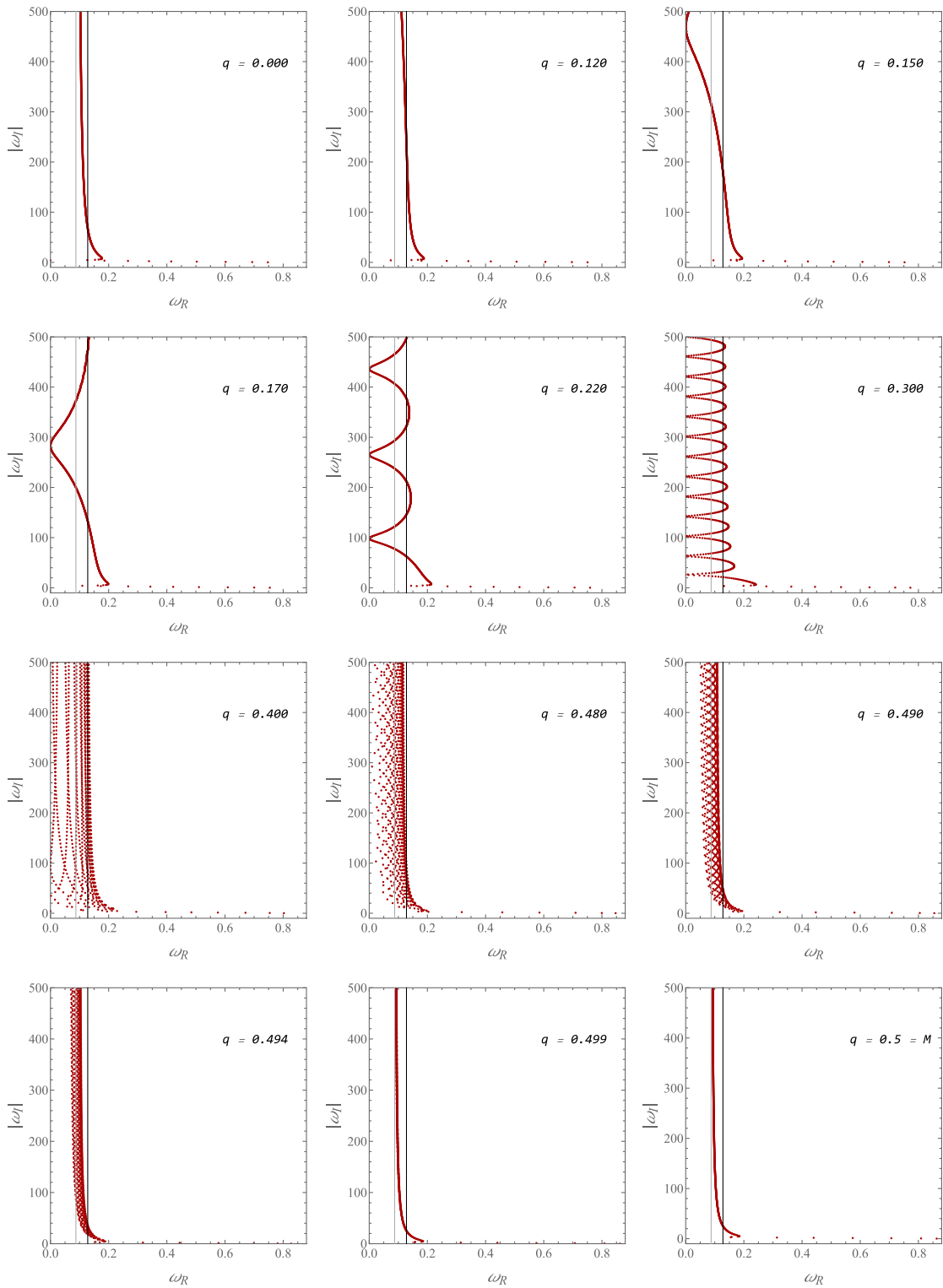
FIG. 1. The QNM spectra for different values of charge with $M = 0.5$ and $\ell = 2$. The light vertical line is at $\omega_R = \ln(3)/(8\pi M)$, and the dark vertical line is at $\omega_R = \ln(5)/(8\pi M)$.

$$C_n = D_{n-1} + \bar{\beta}''_{n-1}B_{n-1} + \hat{\beta}''_{n-2}(A_{n-1} + \bar{\beta}''_{n-1}C_{n-1}),$$
$$n > 2, \tag{3.24}$$

$$D_n = \hat{\alpha}''_{n-2}\bar{\alpha}''_{n-1}\hat{\gamma}''_{n-1}\bar{\gamma}''_n C_{n-1}, \quad n > 2. \tag{3.25}$$

For each n, we can solve Eq. (3.15) for ω. This procedure gives us the same roots as the previous method. However, we find that it is not as efficient in finding the roots. Therefore, the results presented in this paper only use the first method.

IV. NUMERICAL RESULTS

Roots are calculated by Leaver's method [21] (with Nollert's improvement [22]) and are verified by checking that the roots remain stable for different depths in the continued fraction and persist for at least two inversions.

In Fig. 1, we show the QNM spectra for various values of charge q. For all charges there is an initial "bounce" off the imaginary axis at around the ninth mode. Then, for lower values of the charge, there are subsequent bounces starting at some damping rate that decreases with increasing charge.[4] The rough overall picture is that the bounces become more frequent as the charge increases and start lifting away from the imaginary axis. In Fig. 1, this lifting becomes visible at $q = 0.48$. This lifting continues until there is no bouncing at the extremal case. As the charge approaches the extremal limit, the peaks in between the bounces approach $\ln(3)/(8\pi M)$ as damping increases. When the charge approaches zero, the peaks approach $\ln(5)/(8\pi M)$.

To study the asymptotic behavior of the extremal QNM spectrum, we fit the points $(x, y) = (\omega_I, \omega_R)$ with functions of the form

$$y(x) = \frac{a_0 + a_1 x + \cdots + a_n x^n}{b_0 + b_1 x + \cdots + b_n x^n}. \tag{4.1}$$

We then take the limit as $x \to -\infty$ [i.e., $y(x \to -\infty) = a_n/b_n$] to find the asymptotic value of ω_R. For the extremal case, we found that the best fit is a seventh-order rational function and the limit is within 0.0009 of $\ln(3)/(8\pi M)$. From Fig. 1, one can see that the peaks of the bounces make a transition from $\ln(5)/(8\pi M)$ to $\ln(3)/(8\pi M)$ as q approaches M. We looked at the asymptotic behavior of the peak of the bounces for $q = 0.35$ and 0.45. For $q = 0.45$, we found that the best fit is a second-order rational function, and the limit is 0.008 less than $\ln(5)/(8\pi M)$. For $q = 0.35$, we found that the best fit is a fourth-order rational function, and the limit is 0.0003 more than $\ln(5)/(8\pi M)$. Therefore, it appears that the peaks of the bounces make a transition from $\ln(5)/(8\pi M)$

---

[4]For most cases, the bounces do not actually hit the imaginary axis.
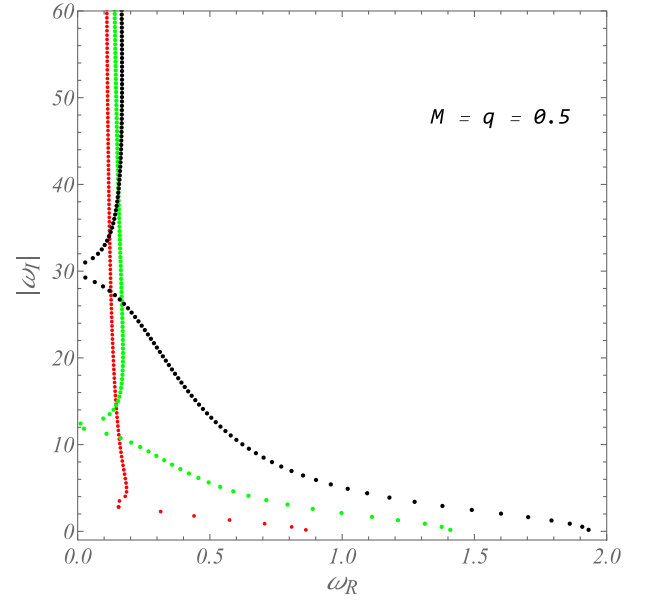

FIG. 2. The QNM low-damped spectra in the extremal cases for, from left to right, $\ell = 2$, 3, 4.

to $\ln(3)/(8\pi M)$ in the charge range of $0.35 \lesssim q < 0.5$. This is consistent with the results in [11].

Our results show that, as the charge gets smaller, the second bounce occurs at approximately $2M^3/q^4$, which is consistent with Eq. (1.2). However, we cannot determine if for very small charges there are no subsequent bounces in transitioning from $\ln(3)/(8\pi M)$ to $\ln(5)/(8\pi M)$, as predicted by the semianalytic calculations of [18].

We also looked at the extremal cases for $\ell = 3$ and 4. The results are shown in Figs. 2 and 3, and in Table I. Again, to determine the asymptotic value, we fit a rational function to the data and found the limit to be within 0.002 of $\ln(3)/(8\pi M)$ for $\ell = 3$ and within 0.004 for $\ell = 4$.

Modes with $\omega_R = 0$ are called algebraically special modes and were discovered analytically by Chandrasekhar [23]. They can be found using the formula given by Berti in [11][5]:

$$\omega = \pm i \frac{(\ell-1)\ell(\ell+1)(\ell+2)}{2[3M + (-1)^s\sqrt{9M^2 + 4q^2(\ell-1)(\ell+2)}]}. \tag{4.2}$$

For gravitational perturbations, where $s = 2$, the above equation gives $\omega_{\ell=2} = -3i$, $\omega_{\ell=3} = -12i$, and $\omega_{\ell=4} = -30i$ when $M = q = 0.5$. Unfortunately, roots near the imaginary axis are numerically difficult to calculate due to the need for higher depth in the continued fraction of Eq. (3.6). For $\omega_{\ell=2}$, Berti found $-3.047876i$, but we were unable to find this, hence the question mark in Table I. In Fig. 2, the gap between neighboring roots for $\omega_{\ell=2}$ seems insufficient to house another root near $-3i$. In the $\ell = 3$ case, the closest root we found to the algebraically special

---

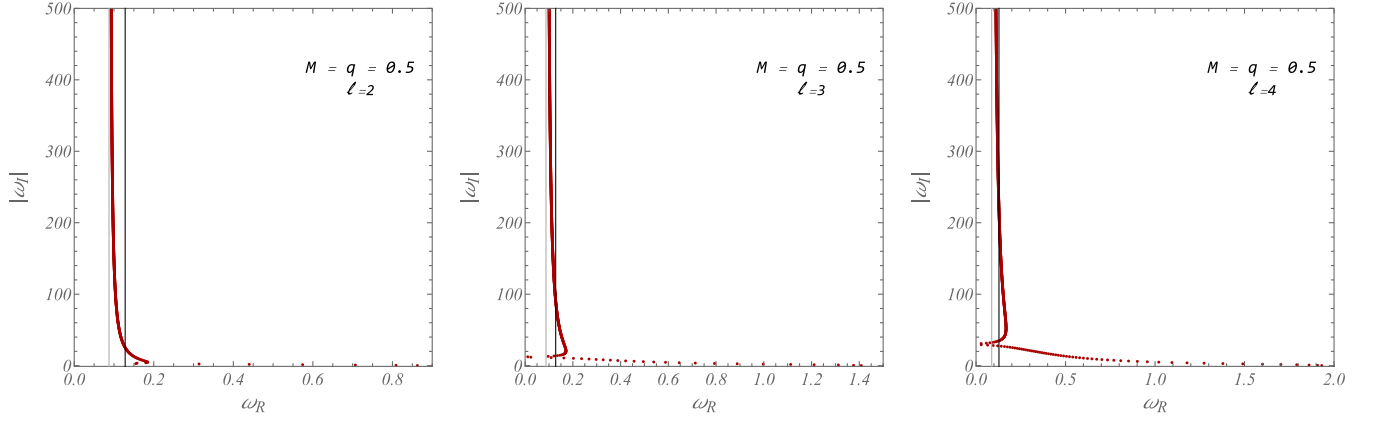[5]This corrects a typo in Eq. (24) of [11].

FIG. 3. The QNM spectra in the extremal cases for, from left to right, $\ell = 2, 3, 4$. The light vertical line is at $\omega_R = \ln(3)/(8\pi M)$, and the dark vertical line is at $\omega_R = \ln(5)/(8\pi M)$.

frequency was $0.01101539 - 12.42338i$. We were unable to find $\omega_{\ell=4}$. However, in Fig. 2, there is a big gap between the two neighboring roots around $\omega_{\ell=4} = -30i$, which suggests there should be another root in this area. See Ref. [11] for discussions regarding the algebraically special frequencies.

V. CONCLUSIONS

Because there have been conflicting results in the literature regarding the asymptotic behavior ($|\omega_I| \to \infty$) of the QNM spectrum of extremal Reissner-Nordström black holes, we numerically calculated over 1000 roots for multipole indices $\ell = 2, 3,$ and 4 using a modification of the continued fraction method. We determined, for all of these indices, the highly damped limit of the real part of the QNMs in the extremal case to be $\ln(3)/(8\pi M)$, consistent with the extremal limit of the nonextremal case. This agrees with the analytic result found in [16].

We also examined the behavior of the spectrum in the nonextremal case for $\ell = 2$. Here, the spectrum has a "bouncing" behavior. The peaks of the bounces asymptotically appear to approach $\ln(5)/(8\pi M)$ for small values of charge, but then transition to $\ln(3)/(8\pi M)$ as the charge becomes larger. In the limit where charge goes to zero, Ref. [18] shows that the spectrum approaches $\ln(3)/(8\pi M)$ in an intermediate damping region and then bounces once and transitions to $\ln(5)/(8\pi M)$ in the high-damping limit. While our results are consistent with this behavior, we were not able to compute enough roots to confirm it.

TABLE I. Gravitational QNMs for the extremal case $q = M = 0.5$ and different values of ℓ.

n	$\ell = 2$	$\ell = 3$	$\ell = 4$
1	$0.8626816 - 0.1669206i$	$1.408445 - 0.1717481i$	$1.931525 - 0.1740026i$
2	$0.8090471 - 0.5099687i$	$1.376931 - 0.5192489i$	$1.907624 - 0.5242399i$
3	$0.7068025 - 0.8827452i$	$1.307249 - 0.8362094i$	$1.860405 - 0.8812876i$
4	$0.5742327 - 1.304909i$	$1.210897 - 1.279042i$	$1.791303 - 1.249989i$
5	$0.4398891 - 1.777137i$	$1.112650 - 1.673036i$	$1.703111 - 1.635329i$
6	$0.3137466 - 2.280441i$	$0.9974355 - 2.117280i$	$1.600492 - 2.041800i$
7	$0.1547576 - 2.806363i$	$0.8886952 - 2.590614i$	$1.489995 - 2.472200i$
8	$-3i$ (?)	$0.7935161 - 3.084178i$	$1.379015 - 2.926427i$
9	$0.1580074 - 3.505822i$	$0.7130847 - 3.589352i$	$1.273919 - 3.401330i$
10	$0.1798750 - 4.033519i$	$0.6455107 - 4.100264i$	$1.178613 - 3.891979i$
25	$0.1537770 - 11.63929i$	$0.0238001 - 11.83155i$	$0.5586342 - 11.56845i$
50	$0.1291992 - 24.18044i$	$0.1689169 - 24.58826i$	$0.2298217 - 24.21602i$
100	$0.1135335 - 49.20611i$	$0.1459628 - 49.64689i$	$0.1671020 - 48.56283i$
250	$0.1014775 - 124.2261i$	$0.1204621 - 124.6934i$	$0.1446396 - 123.6476i$
500	$0.0961954 - 249.2349i$	$0.1083683 - 249.7141i$	$0.1248627 - 248.6851i$
750	$0.0941383 - 374.2385i$	$0.1033898 - 374.7226i$	$0.1162330 - 373.7004i$
1000	$0.0929643 - 499.2405i$	$0.1005974 - 499.7273i$	$0.1112799 - 498.7090i$

[1] B. P. Abbott *et al.* (LIGO Scientific and Virgo Collaborations), Observation of gravitational waves from a binary black hole merger, Phys. Rev. Lett. **116,** 061102 (2016).

[2] S. Hod, Bohr's correspondence principle and the area spectrum of quantum black holes, Phys. Rev. Lett. **81,** 4293 (1998).

[3] M. Maggiore, Physical interpretation of the spectrum of black hole quasinormal modes, Phys. Rev. Lett. **100,** 141301 (2008).

[4] J. Babb, R. G. Daghigh, and G. Kunstatter, Highly damped quasinormal modes and the small scale structure of quantum corrected black hole exteriors, Phys. Rev. D **84,** 084031 (2011).

[5] C. W. Misner, K. S. Thorne, and J. A. Wheeler, *Gravitation* (Freeman, San Francisco, 1973).

[6] S. W. Hawking, G. Horowitz, and S. Ross, Entropy, area, and black hole pairs, Phys. Rev. D **51,** 4302 (1995).

[7] C. Teitelboim, Action and entropy of extreme and nonextreme black holes, Phys. Rev. D **51,** 4315 (1995); **52,** 6201 (E) (1995).

[8] G. Gibbons and C. Hull, A Bogomolny bound for general relativity and solitons in $N = 2$ supergravity, Phys. Lett. **109B,** 190 (1982); R. Kallosh, Supersymmetric black holes, Phys. Lett. B **282,** 80 (1992).

[9] H. Onozawa, T. Mishima, T. Okamura, and H. Ishihara, Quasinormal modes of maximally charged black holes, Phys. Rev. D **53,** 7033 (1996).

[10] H. Onozawa, T. Okamura, T. Mishima, and H. Ishihara, Perturbing supersymmetric black holes, Phys. Rev. D **55,** R4529 (1997).

[11] E. Berti, Black hole quasinormal modes: Hints of quantum gravity?, Conf. Proc. C **0405132,** 145 (2004).arXiv:gr-qc/0411025.

[12] N. Andersson and C. J. Howls, The asymptotic quasinormal mode spectrum of non-rotating black holes, Classical Quantum Gravity **21,** 1623 (2004).

[13] S. Das and S. Shankaranarayanan, High-frequency quasinormal modes for black holes with generic singularities, Classical Quantum Gravity **22,** L7 (2005).

[14] J. Natario and R. Schiappa, On the classification of asymptotic quasinormal frequencies for d-dimensional black holes and quantum gravity, Adv. Theor. Math. Phys. **8,** 1001 (2004).

[15] L. Motl and A. Neitzke, Asymptotic black hole quasinormal frequencies, Adv. Theor. Math. Phys. **7,** 307 (2003).

[16] R. G. Daghigh and M. Green, The highly damped quasinormal modes of extremal Reissner-Nordström and Reissner–Nordström–de Sitter black holes, Classical Quantum Gravity **25,** 055001 (2008).

[17] R. P. Macedo, J. L. Jaramillo, and M. Ansorg, Hyperboloidal slicing approach to quasinormal mode expansions: The Reissner-Nordström case, Phys. Rev. D **98,** 124005 (2018).

[18] R. G. Daghigh, G. Kunstatter, D. Ostapchuk, and V. Bagnulo, The highly damped quasinormal modes of d-dimensional Reissner-Nordström black holes in the small charge limit, Classical Quantum Gravity **23,** 5101 (2006).

[19] S. Chandrasekhar, *The Mathematical Theory of Black Holes* (Clarendon, Oxford, 1983).

[20] E. W. Leaver, Quasinormal modes of Reissner-Nordström black holes, Phys. Rev. D **41,** 2986 (1990).

[21] E. W. Leaver, An analytic representation for the quasinormal modes of Kerr black holes, Proc. R. Soc. A **402,** 285 (1985).

[22] H.-P. Nollert, Quasinormal modes of Schwarzschild black holes: The determination of quasinormal frequencies with very large imaginary parts, Phys. Rev. D **47,** 5253 (1993).

[23] S. Chandrasekhar, On algebraically special perturbations of black holes, Proc. R. Soc. A **392,** 1 (1984).